arXiv:1612.03581v1 [cond-mat.soft] 12 Dec 2016

Microparticle assembly pathways on lipid membranes

Casper van der Wel[1], Doris Heinrich[1, 2], and Daniela J. Kraft[1, *]

[1]Biological and Soft Matter Physics, Huygens-Kamerlingh Onnes Laboratory, Leiden University, PO Box 9504, 2300 RA Leiden, The Netherlands

[2]Fraunhofer Institute for Silicate Research, Neunerplatz 2, 97082 Würzburg, Germany

[*]To whom correspondence should be addressed. E-mail: kraft@physics.leidenuniv.nl

November 28, 2016

Abstract

Understanding interactions between microparticles and membranes of living cells is vital for many applications as well as for unraveling their influence on our health and the environment. Here, we study how microparticles interact with model lipid membranes and each other solely due to a short-ranged adhesive force between membrane and particles. Using confocal microscopy, we establish that above a critical adhesion energy particles first attach to the membrane, then become wrapped, and finally may induce membrane tubulation. The microparticle adhesion state affects the mobility of the particle through a varying drag force that is imposed by the membrane, which is caused by variation in the density and spatial distribution of the membrane-particle linkages. We subsequently categorize the assembly pathways of attached and wrapped microparticles according to whether they are driven by minimization of membrane deformation energy or the strong adhesion energy between membrane and particles. We find that while attached particles do not interact by membrane deformation, they may aggregate when small adhesive vesicles are still present in solution. Only wrapped particles exhibit a reversible attraction that is mediated purely by the deformation of the membrane. When wrapped and non-wrapped particles coexist, they form membrane-mediated dimers that subsequently aggregate into a variety of different structures. The experimental observation of distinct assembly pathways that are only induced by a membrane-particle adhesion shows that microparticles can assemble on lipid membranes even in the absence of a cytoskeleton or other active components.

Introduction

Artificial microparticles are increasingly applied in ceramics, paints, cosmetics, drug delivery [1], and several microbiological techniques such as microrheology [2]. However, the negative environmental effects of polymer-based microparticles, for example through uptake by and high retention in marine organisms, are becoming increasingly clear [3]. In order to be able to unravel the implications of microparticles on health and environment, it is crucial to understand their impact on cellular processes and especially their interactions with the cellular membrane, which is the most important protective barrier of the cell.

The first step in the interaction of microparticles with living cells is their adhesion to the membrane. This adhesion can be caused by a variety of mechanisms such as Van der Waals, Coulomb or hydrophobic forces, or complementary protein interactions [4, 5, 6]. Subsequent internalization into the cell depends on the cell type, the particle size, and the particle surface moieties [6, 7, 8]. As most research has focused on cellular particle uptake, little is known about the organization and dynamics of particles that stay adhered to the membrane. Using vesicles as model cells, membrane-associated microparticles have been observed to exhibit a range of different behaviors, such as lateral diffusion, a long ranged attraction due to membrane deformation, aggregation, and crystal formation [9, 10, 11, 12]. However, a coherent picture describing these collective effects of microparticles on lipid membranes is still lacking.

In order to categorize and systematically describe the multitude of observed interaction processes, we here employ a well-controlled model system of phospholipid Giant Unilamellar Vesicles and microparticles that controllably interact via a complementary protein interaction [12]. We study the microparticle adhesion on lipid membranes with confocal microscopy, which enables us to visualize the particle attachment, membrane deformation, and subsequent assembly pathways. With this system, we characterize three distinct states of the adhesion of individual spherical particles on membranes: attached, wrapped, and tubulated. By measuring the mobility of attached and wrapped particles, we establish that the size of the adhesion patch differs per particle.

The state of individual particles determines the possible interactions between particles: wrapped particles interact via long ranged forces mediated by membrane deformation, attached particles can stick together via small adhesive vesicles, and wrapped and attached particles form dimers driven by the strong membrane-particle adhesion. These membrane-mediated assembly pathways in absence of any active processes point towards a general microparticle aggregation mechanism on cellular membranes.

Materials and Methods

Chemicals

D-glucose (99%), sodium phosphate (99%), deuterium oxide (70%), N-hydroxysulfosuccinimide sodium salt (98%, Sulfo-NHS), and 1,3,5,7-tetramethyl-8-phenyl-4,4-difluoro-bora-diaza-indacene (97%, BODIPY) were acquired from Sigma-Aldrich; methoxypoly(ethylene) glycol amine (mPEG, $M_w = 5000$) from Alfa Aesar; sodium chloride (99%) and sodium azide

(99%) from Acros Organics; 1-ethyl-3-(3-dimethylaminopropyl) carbodiimide hydrochloride (99%, EDC) from Carl Roth; NeutrAvidin (avidin) from Thermo Scientific; DNA oligonucleotides (biotin-5'-TTTAATATTA-3'-Cy3) from Integrated DNA Technologies; Δ9-cis 1,2-dioleoyl-*sn*-glycero-3-phosphocholine (DOPC), 1,2-dioleoyl-*sn*-glycero-3-phosphoethanolamine-N-[biotinyl(polyethylene glycol)-2000] (DOPE-PEG-biotin), and 1,2-dioleoyl-*sn*-glycero-3-phosphoethanolamine-N-(lissaminerhodamine B sulfonyl) (DOPE-rhodamine) from Avanti Polar Lipids. All chemicals were used as received. Deionized water is used with 18.2 MΩcm resistivity, obtained using a Millipore Filtration System (Milli-Q Gradient A10).

Model system

The here employed model system of Giant Unilamellar Vesicles (GUVs) and adhered microparticles builds on earlier work described in ref. [12]. GUVs with diameters ranging from 5 to 20 µm were prepared with electroformation in a 100 mM glucose solution starting from a mixture of 97.5 wt % DOPC, 2.0 wt % DOPE-PEG-biotin, and 0.5 wt % DOPE-rhodamine. To separate the GUVs from smaller lipid vesicles, we filter the solution using a Whatmann 5.0 µm pore size cellulosenitrate filter [13]. Fluorescent polystyrene microparticles (diameter 0.98 ± 0.03 µm) were synthesized in a surfactant-free radical polymerization [14]. To ensure a specific and strong adhesion between the microparticles and the lipid membrane we coated the microparticles with avidin and mPEG, using an EDC/Sulfo-NHS coating procedure. Per 15 mg particles, 15–50 µg NeutrAvidin and 4.0 mg mPEG were added. Sodium azide was added to a concentration of 3 mM to prevent bacterial growth. The density of biotin binding sites was quantified using a fluorescence assay with DNA oligonucleotides having a biotin and a fluorescent marker [12].

Avidin is known to bind specifically to biotin, a process that occurs spontaneously when mixing 20 µL of the GUVs with 0.04 µg microparticles in a phosphate buffered saline solution (PBS, pH=7.4) that was density-matched to the particles using heavy water. The PBS had the same osmolarity as the 100 mM glucose inside the GUV. After an incubation time of 10 min, the GUV-particle mixture was distributed into a microscope sample holder containing 50 µL of PBS.

In order to obtain tense vesicles ($\sigma > 1\,\mu\mathrm{N\,m^{-1}}$) this sample was closed directly to prevent the evaporation of water. To obtain floppy vesicles, the sample was imaged without closing the sample holder, allowing water to evaporate from the sample. Evaporation increases the osmolarity of the outside solution without any osmotic shocks on the vesicles so that vesicles gradually deflate. For floppy vesicles, the corresponding membrane tension was below $10\,\mathrm{nN\,m^{-1}}$, as confirmed by a membrane fluctuation analysis [15]. As the membrane-particle linkage is essentially irreversible, the particles stay wrapped even when the membrane tension increases afterwards.

Diffusion measurements

Diffusion measurements of membrane-attached particles were performed by imaging the top part of a tense GUV with attached particles (see Figure S1). The particle trajectories were extracted from the recorded image sequences using Trackpy [16]. Simultaneously, the fluorescence signal of the top part of the vesicle was recorded. The center of the vesicle

was extracted from a two-dimensional Gaussian fit of this fluorescence and, using a separate measurement of the vesicle size, the full three-dimensional coordinates of the particles could be reconstructed [17].

As membrane-wrapped particles tend to interact with other particles (see Results section), diffusion measurements of these particles required continuous confirmation of the wrapped state. Therefore, these measurements were performed on image sequences of the equatorial plane of a particle-covered GUV (see Figure S2). The particle coordinates were extracted in the same way as for the attached particles. The vesicle position was determined by fitting circles to the vesicle contour [17]. Together with a separate measurement of the vesicle size, this yielded the full three-dimensional coordinates of the particles.

The diffusion coefficient was measured from the one-dimensional mean squared displacement along the vesicle contour. As the tracked particles could freely move out from the equatorial plane, this limited the length of the particle tracks and thus increased the uncertainty in the single-particle diffusion coefficients. Particles that were closer than 2.5 µm to other particles were omitted to rule out many-particle effects [12]. The diffusion coefficient was measured for each particle separately with linear regression of the mean squared displacements. As particles were confined to a spherical surface, the mean squared displacement only grows linearly in time if the squared curvature R^2 is much larger than the measured mean squared displacement [18]. In order to meet this condition, we limited the displacement measurements to short time intervals up to 4 frames, corresponding to maximum lag times of 35–70 ms.

Imaging

Samples were imaged with a Nikon Ti-E A1R confocal microscope equipped with a 60× water immersion objective (NA = 1.2). To enable fluorescence imaging, the particles were loaded with BODIPY, and the GUVs were doped with 0.5 wt % DOPE-rhodamine. The coverslips were coated with a layer of polyacrylamide to prevent particle adhesion. High-speed images used in the diffusion measurements were recorded at 57–110 Hz using a horizontal resonant scanning mirror, while high-resolution close-ups were recorded with a set of Galvano scanning mirrors.

Results and Discussion

Polymer microparticles can adhere to lipid membranes by various kinds of (bio)chemical interactions [4, 5, 6]. In our experiments, we established adhesion in a controlled manner by an avidin-biotin interaction: the particles are coated with the protein avidin and the membranes include a biotinylated lipid. Once connected to a membrane, particles do not detach due to the high energy associated with the non-covalent linkage between biotin and avidin (approx. 17 k_BT [19], with k_BT being the thermal energy), and the possibility of forming multiple connections (see Figure 1). Previously, it was established that the membrane fully wraps around the microparticle if the membrane-particle adhesion energy per unit area u_{ad} exceeds the cost for membrane bending $2\kappa R^{-2}$ and membrane tension σ [20, 21, 22, 23, 12]. Here R denotes the particle radius and κ the membrane bending rigidity.

We tune the adhesion state by adjusting the energy through the density of biotin binding sites on the particles. Below a critical density of $513 \pm 77\,\mu\text{m}^{-2}$, the membrane does not deform under the influence of microparticle adhesion (see Figure 1*A*-*C*). Above the critical linker density and in the limit of low surface tension, $u_{ad} > 2\kappa R^{-2} \gg \sigma$, particles are fully wrapped and connected to the membrane only by a "neck region" (see Figure 1*D*-*F*). The shape of this region is predicted to be catenoidal by the Canham-Helfrich model [22]. At high membrane tension, particles do not induce membrane deformation, at least up to the optical resolution limit [12].

In this article, we will investigate the dynamics of particles in the attached and the wrapped states and their assembly behavior. We will first probe the membrane adhesion of isolated particles by measuring the influence of the membrane on the particle mobility. Then, we will map out the assembly pathways of multiple particles that lead to membrane-mediated configurations. Finally, we will investigate spontaneous tubulation that occurs at particle inclusions.

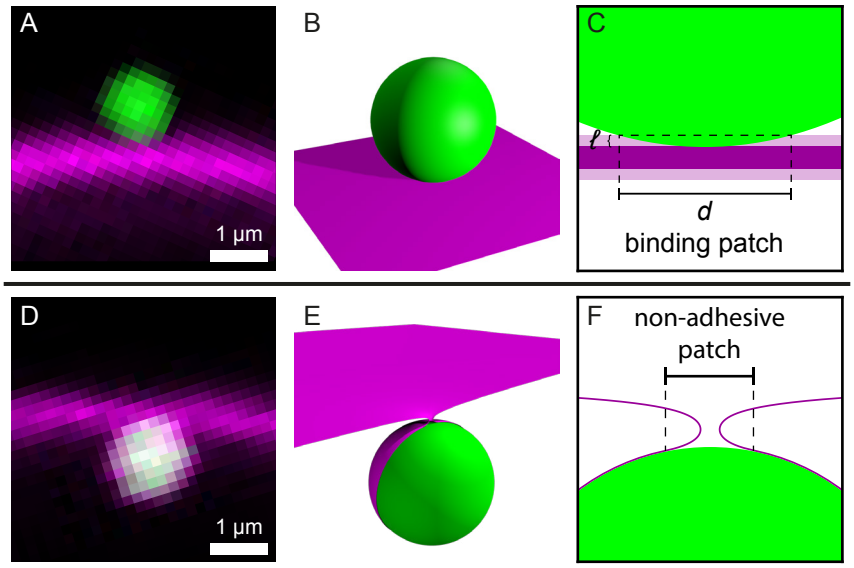

Figure 1: Attached and wrapped states of membrane-adhered microparticles. (*A*) A high-resolution confocal slice and (*B*) a schematic of a colloidal particle (green) attached to a lipid membrane (magenta) is shown. In (*C*) a close-up of the binding patch with diameter d is depicted, where the estimated maximum membrane linking distance $\ell = 2\,\text{nm}$ is represented as a shaded region on top of the membrane. The illustration was compressed in the horizontal direction by a factor 3. (*D*) A confocal image and (*E*) the corresponding illustration of a membrane-wrapped particle. The white color of the particle is caused by the overlap of the fluorescence of the particle itself and the membrane surrounding it. The cross-section of the binding area and catenoidal shaped neck region are displayed in (*F*). The membrane thickness is depicted to scale with the particle size. We arbitrarily chose a non-adhesive patch size for the purpose of illustrating the wrapped state.

Mobility of membrane-associated particles

While a particle retains its lateral mobility when it adheres to a liquid lipid membrane, the Brownian motion of the particle changes from three-dimensional to two-dimensional. Therefore its mean squared displacement changes from $\langle x^2 \rangle = 6Dt$ in the freely dispersed case to $4Dt$ in the bound case, where D is the diffusion coefficient and t denotes the lag time over which $\langle x^2 \rangle$ is measured. From the Saffman-Delbrück equations [24] we expect that upon particle adhesion its diffusion coefficient is lowered significantly due to an additional drag force caused by the relatively high viscosity of the membrane. The particle mobility is then related to the effective patch size of the membrane that is forced to move along with the particle [24, 25].

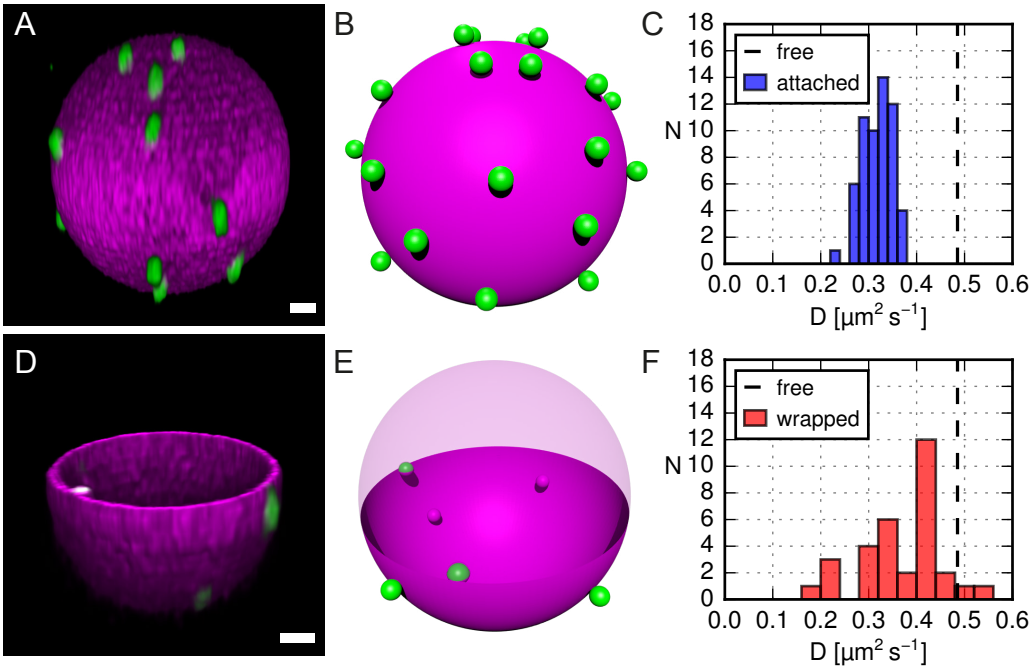

Figure 2: Diffusion coefficients of membrane-adhered particles. In (A), a three-dimensional reconstruction of a confocal image with particles attached to a vesicle is shown (scalebar 2 µm), with the corresponding illustration in (B). A histogram of single-particle diffusion coefficients of these attached particles is shown in (C). Here, only coefficients with a standard error below $0.02\,\mu m^2\,s^{-1}$ were included. In (D), one hemisphere of a membrane with one wrapped and two attached particles is displayed (scalebar 2 µm), with (E) the corresponding illustration, and (F) the histogram of single-particle diffusion coefficients. Here, only diffusion coefficients with a standard error below $0.1\,\mu m^2\,s^{-1}$ were included. For reference, the diffusion coefficient of freely dispersed particles is displayed by a dashed black line in (C) and (F).

For the diffusion measurements of attached particles, we used particles with biotin binding site densities ranging from 5×10^1 to $1.5 \times 10^3\,\mu m^{-2}$ adhered to membranes with a surface tension above $1\,\mu N\,m^{-1}$. This high choice of the membrane tension ensured that particles were not wrapped (see Figure 2A). As a reference, we first measured the diffusion constant

of freely suspended particles and found it to be $0.48\,\mu m^2\,s^{-1}$. Then, from 58 trajectories with an average length of 2290 frames, we obtained a distribution of the single-particle diffusion coefficients after membrane attachment, as shown in Figure 2*C*. Compared to freely suspended particles, the diffusion coefficient lowered to $0.32 \pm 0.05\,\mu m^2\,s^{-1}$. Furthermore, we observed a significant difference between individual particles. This spread in the diffusion coefficients is not due to a measurement imprecision, as we omitted single-particle diffusion coefficients with an estimated standard error above $0.02\,\mu m^2\,s^{-1}$ [26, 27]. Thus, we conclude that the membrane imposes a drag that differs per particle.

Although we observed a spread in the distribution of single-particle diffusion coefficients, there was no apparent difference in the particle-membrane adhesion distinguishable in the confocal microscopy images. Within the optical resolution limit, all particles were observed not to deform the membrane, which is in accordance with the theoretical prediction when the membrane tension σ is larger than the membrane-particle adhesion per unit area u_{ad}. Still, even without any membrane deformation, the binding patch may differ from particle to particle. The finite distance between the membrane and biotin gives rise to a binding patch diameter d set by the linker length ℓ and the particle radius R via $d = 2\sqrt{R^2 - (R-\ell)^2}$. If we estimate ℓ to be 2 nm, which is based on the size of a PEG2000 spacer [28, 29], the associated binding patch diameter d is 90 nm, as illustrated in Figure 1*C*. Within this potential binding area, multiple links can be formed without deforming the membrane, due to the flexibility of the PEG spacer. A variation the concentration or spatial distribution of avidin on the particle, and thus the number of bound lipids that are forced to diffuse with the particle, likely leads to the observed spread in particle mobility. Unfortunately, we cannot infer a particle-bound membrane patch size using the Saffman-Delbrück equations from the observed mobility of membrane-attached particles [24], such as is appropriate for smaller membrane-adhered objects [30]. The reason for this is that the motion of the particle is governed by both the bulk liquid and the membrane, which is apparent from the observation that the diffusivity of freely diffusing particles is on the same order of magnitude as the attached particles [31, 32].

We measured the diffusion of wrapped particles using a single batch of particles with biotin binding site densities between 1.3×10^2 and $1.5 \times 10^3\,\mu m^{-2}$ (see Figure 2*D-E*). To ensure a wrapped fraction of particles of 60%, we increased the available membrane surface area by lowering the tension of the GUVs temporarily below $10\,nN\,m^{-1}$ [12]. We measured 35 trajectories with an average length of 153 frames; the maximum error in these measurements was $0.1\,\mu m^2\,s^{-1}$. As can be seen in Figure 2*F*, again the membrane association lowered the diffusivity of the particles. However, the observed spread in the diffusion coefficients was even larger than the spread for attached particles: some particles exhibited a diffusion coefficient close to that of freely suspended particles, while others experienced up to a three-fold decrease. We presume that the reduced mobility of wrapped particles is caused by the neck region that connects particle and membrane, and not by the membrane region that is wrapped around the particle. Although we cannot observe any differences in this neck region between individual particles, there likely is a variation in the neck size that is below the resolution of the microscope (approximately 200 nm). We hypothesize that this neck size is determined by a non-adhesive patch on the particle (see Figure 1*F*). This non-adhesive patch is likely caused by the finite number of particle-attached linkers: for the here employed maximum linker density of $1.5 \times 10^3\,\mu m^{-2}$, the average distance between linkers is 26 nm,

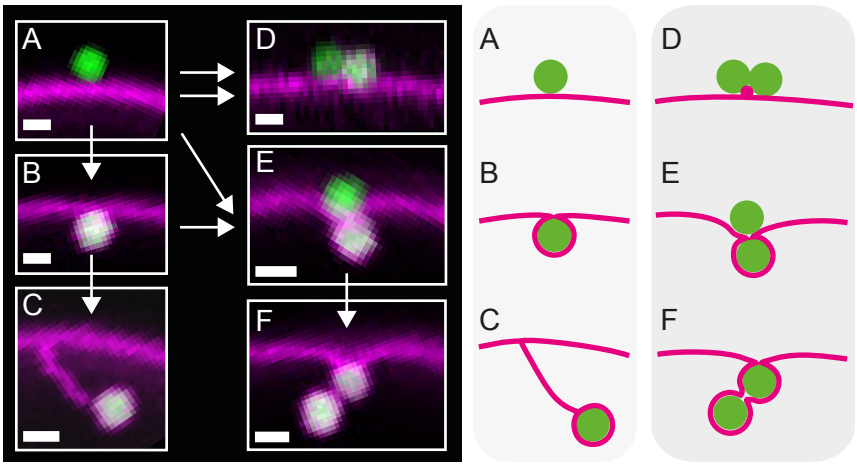

Figure 3: Membrane-mediated irreversible assembly pathways of microparticles, displayed in confocal images (left, scale bars: 1 µm) and sketches (right). White arrows denote particle assembly pathways. A membrane-attached particle *(A)* is wrapped at large membrane-particle adhesion energy and low membrane tension *(B)*. This particle can induce the formation of a membrane tube (*C*, see also Movie S1). *(D)* Two non-wrapped particles can stick together via a secondary lipid vesicle. *(E,F)* A non-wrapped particle assembles with a wrapped particle forming a membrane-mediated dimer *(E)* that is subsequently fully wrapped by the membrane *(F)*.

whereas for the critical linker density for wrapping of $0.5 \times 10^3\,\mu\text{m}^{-2}$ this distance is 45 nm. Another reason for the presence of a non-adhesive patch could be the adsorption of small vesicles on the particle surface. This would locally occupy linkers which can subsequently not connect to the GUV membrane anymore, thereby effectively creating a non-adhesive patch that also sets the particle-induced neck size.

To summarize, membrane-attached particles do not deform the membrane, but still experience a varying membrane-imposed drag through variations in the number of membrane-particle linkages. Wrapped particles also experience a varying drag, but now governed by the size of a non-adhesive patch on the particle, which may again be determined by the finite density of particle-attached linkers, or adsorption of small secondary lipid structures on the particle that inhibit a patch of linkers. Therefore, a spread in the linker concentration, or the presence of small lipid vesicles, results in a variation in the microscopic nature of the membrane-particle linkage. The here described diffusion measurements revealed a significant spread in the particle dynamics, which may affect the timescales of the assembly pathways that are described in the next section.

Furthermore, the observed spread in the diffusivity of wrapped particles implies a variation in the particle-induced membrane deformation and thus may have consequences for the long ranged attraction between membrane-deforming particles that was quantified previously [12]. In order to precisely measure the effect of the particle-induced deformation on particle mobility and interaction, an accurate control over the neck size is required. This might be achieved using asymmetric "Janus" particles that have a controlled non-adhesive patch size [33].

Microparticle assembly pathways

The two states of particle-membrane adhesion, attached to and wrapped by the membrane, potentially lead to different interactions. In previous experiments, observations of a long-ranged membrane deformation-mediated attraction have been described [9] and later quantified [11, 12], while also different phenomena such as permanent aggregation or crystallization have been reported [10, 12]. The underlying mechanisms have been conjectured to be a long-ranged membrane-bending mediated force and a short-ranged adhesion mediated force. However, a connection between the particle-membrane state, the involved type of force and resulting assembly pathway has not been established yet. In order to develop a coherent picture, we will here employ confocal microscopy to systematically study the interaction pathways between all combinations of single-particle adhesion states: (1) wrapped-wrapped, (2) attached-attached, and (3) wrapped-attached.

Two membrane-wrapped particles (Figure 3*B*) exhibit a long ranged interaction that has been described extensively in theory and simulation [34, 35, 36], and only recently quantified by experiments. In these experiments, the interaction has been reported to be attractive with a strength ranging from $3\,k_BT$ [12] to $100\,k_BT$ [11]. Despite the large difference in the absolute attraction strength, the observed interaction extends in both cases over several micrometers and has therefore been attributed to membrane deformation. On the other hand, membrane-attached particles (Figure 3*A*) have been shown to not interact with each other via a deformation-mediated interaction [12].

Next to these known assembly pathways, we observed a third possibility when a wrapped particle encountered an attached particle: the local deformation of the membrane induced by the wrapped particles can serve as a binding site for attached particles (Figure 3*E* and 4). This phenomenon was observed each time when an attached particle came in contact with a wrapped particle. Attached particles were captured irreversibly due to the increased contact area on top of the wrapped particle (see Figure 4). Although the membrane-particle linkages are mobile in the membrane, the attached particle cannot escape once the linkages are formed in this ring-shaped region. This is because the formed ring of bound linkers would need to cross the central non-binding patch, which requires the breakage of linkages. In this way, the attached particle is topologically protected from detaching from the wrapped particle and diffuse together as a membrane-mediated dimer.

Rarely, we observed a two-step hierarchical wrapping: after formation of the membrane-mediated dimer, the previously attached particle becomes wrapped resulting in a tube-like structure containing two wrapped spheres (see Figure 3*F*). Apparently, the biotin binding sites density on the second particle is large enough to ultimately become fully wrapped, but this only happened after the dimerization upon a further decrease in membrane tension.

In addition to these assembly pathways that are determined by the adhesion state of the particles, we found that the presence of small ($R < 1\,\mu m$) lipid vesicles can also lead to permanent binding between particles (Figure 3*D* and S3). These small vesicles can only be identified by their fluorescence in confocal images, while they are typically invisible in bright field microscopy. This irreversible aggregation has also been observed in previous measurements and hypothesized to originate from a membrane-deformation mediated force, although at that time the presence of small lipid vesicles could not be excluded. While membrane deformation might have induced the reported long-ranged attraction, it remains

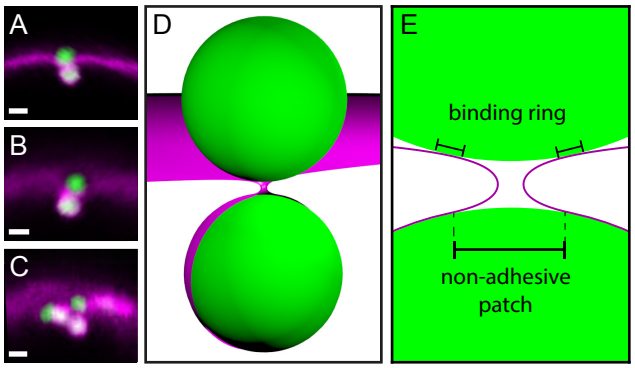

Figure 4: Membrane-mediated dimer of microparticles. *(A)-(B)* High-resolution confocal slices of single dimers and *(C)* a combination of two assembled dimers. The wrapped half of the dimer can be identified by the white color which is caused by the overlap of the membrane and particle fluorescence. The scale bars denote 1 µm. A three-dimensional illustration of the dimer is shown in *(D)*. In *(E)* a cross-section is depicted, showing the bound ring between the membrane and the top particle, which irreversibly connects the particles. The non-adhesive patch size was chosen arbitrarily; the membrane thickness is to scale with the particle diameter.

unclear whether the observed irreversible aggregation was due to membrane deformation or short-ranged adhesion [9, 10]. This aggregation pathway can be suppressed by removing the small lipid vesicles, using for instance filtration [13]. Contrary to the attached particles, fully wrapped particles cannot aggregate via small lipid vesicles, purely for the reason that their surface is already occupied.

Thus, the short-ranged membrane-particle adhesion mechanism drives the lipid vesicle mediated interactions that result in aggregation of attached particles (Figure 3D) as well as in the dimerization of attached and wrapped particles (Figure 3E). These adhesion-driven interactions continue to play a role as long as there is any area on the particle left that is not covered, such as is the case for the attached particles (Figure 3A and D) or for the membrane-mediated dimer (Figure 3E). Indeed, two dimers assembled into membrane-mediated tetramers (Figure 4C), and multiple attached particles aggregated via secondary lipid vesicles. Depending on the particle concentration and waiting time after mixing, particles assembled into permanent aggregates of 5-50 particles (see Figure S3).

In summary, by using confocal microscopy we were able to distinguish a variety of assembled microparticle structures mediated purely by a lipid membrane, either through membrane deformations or the short-ranged adhesive forces between membrane and particles. We correlated the different observed structures with the initial state of wrapping of the individual particles and found three mechanisms for membrane-mediated interactions. Firstly, membrane deformations give rise to long-ranged interactions. Secondly, for a system consisting of non-wrapped particles only, particle aggregates are caused by small ($R < 1$ µm) secondary lipid vesicles. Thirdly, collisions between non-wrapped and wrapped particles lead to permanent membrane-mediated dimers due to the formation of a ring-like binding topology. As long as there is unoccupied area on particles, the strong membrane-particle adhesion force can drive subsequent aggregation of particles. This observation of aggregation on GUVs

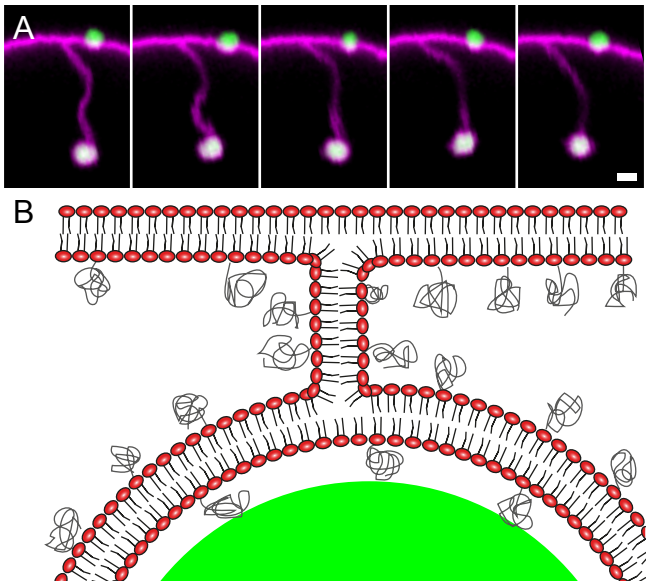

Figure 5: Particle-induced membrane tubulation. (A) A time lapse of five confocal images displaying a particle-induced tube. The time between frames is 127 ms, and the scale bar is 1 µm. The tube fluctuation is clearly visible (see Movie S1 for the corresponding video). In (B) an illustration of the hypothesized particle induced tubular micelle is shown. The lipid-attached PEG2000 molecules are denoted with gray lines. The (green) particle is not to scale with the membrane thickness.

proves that for the formation of membrane-mediated aggregates, no cytoskeleton or other active components are necessary: the adhesion between particle and membrane is sufficient for aggregation.

Spontaneous membrane tubulation

After a particle had been wrapped by the lipid membrane, we occasionally observed spontaneous formation of a membrane tube starting from the neck of the wrapped particle onwards (see Figure 5A and corresponding Movie S1). This process occurred for less than 1 % of all wrapped particles. The particles remained wrapped by and connected to the vesicle membrane, but could freely diffuse in the vesicle interior. The membrane tubes exhibited large thermal fluctuations and we never observed reversal of the tubulation process, which suggests the absence of tensile forces that would retract the particle.

Spontaneous formation of membrane tubes is an ubiquitous process in living cells [37, 38, 39]. However, in our experiments this is only possible if the bilayer would have a preferred curvature. In the absence of such a preferred curvature, it has been established that a supporting force $F = 2\pi\sqrt{2\sigma\kappa}$ is necessary to stabilize membrane tubes against retraction, and that its radius is given by $R = \sqrt{\kappa/(2\sigma)}$ [40, 41, 42]. Taken together, this yields $F = 2\pi\kappa/R$. Since the the membrane diameter of our observed tubes is below the diffraction limit, $R < 100\,\mathrm{nm}$, a tube-supporting tensile force would need to be larger than 5 pN (given $\kappa = 21\,\mathrm{k_B T}$ [43]). Clearly, such a force is absent in our experiments, as the particle diffuses freely after tube-formation for the duration of the experiment. Thus, we conclude that only

a preferred curvature of the bilayer could explain the observed membrane tubes [44].

Such a preferred curvature might be imposed by the design of our specific model membrane: the bulky DOPE-PEG-biotin lipids could be depleted locally from the outer membrane leaflet by binding to particles, thereby creating a leaflet asymmetry and preferred curvature that stabilizes the inward tube formation. However, given the here employed DOPE-PEG-biotin molar fraction of 0.5%, this mechanism seems unlikely. The number of these functionalized lipids per unit area is approximately $8 \times 10^3\,\mu m^{-2}$ [45, pp. 381]. On the one hand, this amount is too low to have any lateral steric interactions between the PEG2000 polymers and thus steric pressure that may lead to an induced curvature [29]. On the other hand, this concentration is too high to induce a sufficient leaflet asymmetry due to the comparatively low binding site density on the particles which only depletes an insignificant fraction of DOPE-PEG biotin lipids on one side of the bilayer.

Therefore we here hypothesize that the observed tube is in fact a rodlike micelle: the tube connecting the particle and the bilayer consists of a monolayer of lipid molecules instead of a bilayer (see Figure 5(B)). This monolayer is formed from the inner leaflet of the vesicle after a spontaneous bilayer rearrangement in the neck region of a wrapped particle. The large energy barrier required for such a rearrangement of the bilayer is overcome by the high curvature of the neck region. After the formation of the micelle-like tube, the overall membrane curvature is lowered and the neck region can be extended and further stabilized by the bulky headgroup of the wedge-shaped DOPE-PEG-biotin [29, 46] and the free energy gain from the additional translational entropy of the particle. In addition, we did not observe any attraction between the tube origin on the GUV and other membrane-attached particles such as is present for wrapped particles. This further suggests that these tubular structures do not deform the outer membrane indicating that the observed structures are rodlike micelles.

Conclusion

We investigated the interaction of adhesive microparticles with lipid membranes and established three distinct particle-membrane configurations. Initially, a particle attaches to the membrane without creating any visible deformation. Subsequently, given that the membrane tension is sufficiently low and the adhesion energy is sufficiently high, the membrane almost fully wraps the particle resulting in a membrane-coated particle. Such a wrapped particle is attached to the membrane via a narrow ($< 200\,nm$) neck region. Finally, this neck region may expand in a tube or rodlike micelle of multiple micrometers that connects the wrapped particle and the membrane.

After adhesion to the membrane, the particles remain laterally mobile on the membrane. We have quantified the particles' mobility and found that their diffusion coefficient of $0.48\,\mu m^2\,s^{-1}$ in dispersion is reduced to $0.32 \pm 0.05\,\mu m^2\,s^{-1}$ after membrane attachment. As there is a significant spread in the measured single-particle diffusion coefficients, we conclude that particles attach with varying number of linkers. For wrapped particles, we observed diffusion coefficients in the range of 0.15–$0.55\,\mu m^2\,s^{-1}$, showing that the neck region connecting particle and membrane is variable in size. We hypothesize that the diameter of the neck region is set by a non-adhesive patch on the particle surface, whose size varies due to the distribution of linkers.

Membrane-associated particles can interact with each other in three ways. Firstly, membrane-wrapped particles interact with each other through a membrane deformation mediated force that ranges over several particle diameters [9, 11, 12]. Secondly, this interaction is not present for attached particles that do not deform the membrane. However, these can irreversibly aggregate via smaller secondary vesicles. Thirdly, attached particles can become trapped in the deformation sites created by a wrapped particle, forming membrane-mediated dimers. The last two adhesion-mediated mechanisms ultimately result in complex random aggregates of multiple particles.

The observed aggregation of colloidal particles mediated by lipid membranes shows that even in the absence of proteins or active components, particles aggregate in order to optimize the contact area with the lipid membrane, or to minimize the membrane deformation. This systematic description of the assembly pathways of microparticles on model lipid membranes will enable a better understanding of the assembly of membrane-associated objects in biological systems, for example the accumulation of microplastics.

Author Contributions

D.J.K. and D.H. designed the project; C.v.d.W. carried out experiments and data analysis supervised by D.J.K. and D.H.; all authors contributed to writing and revising the manuscript.

Acknowledgement

The authors thank Timon Idema for useful discussions and Marcel Winter for support during particle synthesis. This work was supported by the Netherlands Organisation for Scientific Research (NWO/OCW), as part of the Frontiers of Nanoscience program and VENI grant 680-47-431.

References

[1] F. Tang, L. Li, and D. Chen. Mesoporous silica nanoparticles: Synthesis, biocompatibility and drug delivery. *Adv. Mater.*, 24:1504–1534, 2012.

[2] Y. Tseng, T. P. Kole, and D. Wirtz. Micromechanical mapping of live cells by multiple-particle-tracking microrheology. *Biophys. J.*, 83(6):3162–3176, 2002.

[3] M. Cole, P. Lindeque, C. Halsband, and T. S. Galloway. Microplastics as contaminants in the marine environment: A review. *Mar. Pollut. Bull.*, 62:2588–2597, 2011.

[4] A. E. Nel, L. Mädler, D. Velegol, T. Xia, E. M. V. Hoek, P. Somasundaran, F. Klaessig, V. Castranova, and M. Thompson. Understanding biophysicochemical interactions at the nano-bio interface. *Nat. Mater.*, 8:543–557, 2009.

[5] M. Mahmoudi, J. Meng, X. Xue, X. J. Liang, M. Rahman, C. Pfeiffer, R. Hartmann, P. R. Gil, B. Pelaz, W. J. Parak, P. del Pino, S. Carregal-Romero, A. G. Kanaras, and S. Tamil Selvan. Interaction of stable colloidal nanoparticles with cellular membranes. *Biotechnol. Adv.*, 32(4):679–692, 2014.

[6] A. Vonarbourg, C. Passirani, P. Saulnier, and J. P. Benoit. Parameters influencing the stealthiness of colloidal drug delivery systems. *Biomaterials*, 27(24):4356–4373, 2006.

[7] J. Rejman, V. Oberle, I. S. Zuhorn, and D. Hoekstra. Size-dependent internalization of particles via the pathways of clathrin- and caveolae-mediated endocytosis. *Biochem. J.*, 377:159–169, 2004.

[8] M. R. Lorenz, V. Holzapfel, A. Musyanovych, K. Nothelfer, P. Walther, H. Frank, K. Landfester, H. Schrezenmeier, and V. Mailänder. Uptake of functionalized, fluorescent-labeled polymeric particles in different cell lines and stem cells. *Biomaterials*, 27(14):2820–2828, 2006.

[9] I. Koltover, J. O. Rädler, and C. R. Safinya. Membrane mediated attraction and ordered aggregation of colloidal particles bound to giant phospholipid vesicles. *Phys. Rev. Lett.*, 82(9):1991–1994, 1999.

[10] L. Ramos, T.C. Lubensky, N. Dan, P. Nelson, and D. A. Weitz. Surfactant-mediated two-dimensional crystallization of colloidal crystals. *Science*, 286:2325–2328, 1999.

[11] R. Sarfati and E. R. Dufresne. Long-range attraction of particles adhered to lipid vesicles. *Phys. Rev. E*, 94:012604, 2016.

[12] C. van der Wel, A. Vahid, A. Šarić, T. Idema, D. Heinrich, and D. J. Kraft. Lipid membrane-mediated attractions between curvature inducing objects. *Sci. Rep.*, 6:32825, 2016.

[13] Y. Tamba, H. Terashima, and M. Yamazaki. A membrane filtering method for the purification of giant unilamellar vesicles. *Chem. Phys. Lipids*, 164:351–358, 2011.

[14] J. Appel, S. Akerboom, R. G. Fokkink, and J. Sprakel. Facile one-step synthesis of monodisperse micron-sized latex particles with highly carboxylated surfaces. *Macromol. Rapid Comm.*, 34:1284–1288, 2013.

[15] J. Pécréaux, H.-G. Döbereiner, J. Prost, J.-F. Joanny, and P. Bassereau. Refined contour analysis of giant unilamellar vesicles. *Eur. Phys. J. E*, 13:277–290, 2004.

[16] D. B. Allan, T. A. Caswell, N. C. Keim, and C. van der Wel. Trackpy v0.3.0. *Zenodo*, 34028, nov 2015.

[17] C. van der Wel. Circletracking v1.0. *Zenodo*, 47216, 2016.

[18] S. Paquay and R. Kusters. A method for molecular dynamics on curved surfaces. *Biophys. J.*, 110:1226–1233, 2016.

[19] V. T. Moy, E.-L. Florin, and H. E. Gaub. Intermolecular forces and energies between ligands and eeceptors. *Science*, 266:257–259, 1994.

[20] R. Lipowsky, H.-G. Döbereiner, C. Hiergeist, and V. Indrani. Membrane curvature induced by polymers and colloids. *Physica A*, 249:536–543, 1998.

[21] R. Lipowsky and H.-G. Döbereiner. Vesicles in contact with nanoparticles and colloids. *Europhys. Lett.*, 43(2):219–225, 1998.

[22] M. Raatz, R. Lipowsky, and T. R. Weikl. Cooperative wrapping of nanoparticles by membrane tubes. *Soft Matter*, 10:3570–3577, 2014.

[23] J. Agudo-Canalejo and R. Lipowsky. Critical particle sizes for the engulfment of nanoparticles by membranes and vesicles with bilayer asymmetry. *ACS Nano*, 9(4):3704–3720, 2015.

[24] P. G. Saffman and M. Delbrück. Brownian motion in biological membranes. *P. Natl. Acad. Sci. USA*, 72(8):3111–3113, 1975.

[25] B. D. Hughes, B. A. Pailthorpe, and L. R. White. The translational and rotational drag on a cylinder moving in a membrane. *J. Fluid Mech.*, 110:349, 1981.

[26] H. Qian, M. P. Sheetz, and E. L. Elson. Single particle tracking Analysis of diffusion and flow in two-dimensional systems. *Biophys. J.*, 60:910–921, 1991.

[27] D. Ernst and J. Köhler. Measuring a diffusion coefficient by single-particle tracking: statistical analysis of experimental mean squared displacement curves. *Phys. Chem. Chem. Phys.*, 15:845–849, 2013.

[28] P. G. de Gennes. Polymers at an interface; a simplified view. *Adv. Colloid Interfac.*, 27:189–209, 1987.

[29] A. K. Kenworthy, K. Hristova, D. Needham, and T. J. McIntosh. Range and magnitude of the steric pressure between bilayers containing phospholipids with covalently attached poly(ethylene glycol). *Biophys. J.*, 68(5):1921–1936, 1995.

[30] T. T. Hormel, S. Q. Kurihara, M. K. Brennan, M. C. Wozniak, and R. Parthasarathy. Measuring lipid membrane viscosity using rotational and translational probe diffusion. *Phys. Rev. Lett.*, 112:188101, 2014.

[31] A. Naji, A. J. Levine, and P. A. Pincus. Corrections to the Saffman-Delbrück mobility for membrane bound proteins. *Biophys. J.*, 93(11):L49, 2007.

[32] H. A. Stone and H. Masoud. Mobility of membrane-trapped particles. *J. Fluid Mech.*, 781:494–505, 2015.

[33] N. Li, N. Sharifi-Mood, F. Tu, D. Lee, R. Radhakrishnan, T. Baumgart, and K. J. Stebe. Curvature-driven migration of colloids on lipid bilayers. *arXiv*, 1602.07179, 2016.

[34] K. S. Kim, J. Neu, and G. Oster. Curvature-mediated interactions between membrane proteins. *Biophys. J.*, 75:2274–2291, 1998.

[35] B. J. Reynwar and M. Deserno. Membrane-mediated interactions between circular particles in the strongly curved regime. *Soft Matter*, 7:8567, 2011.

[36] A. Šarić and A. Cacciuto. Fluid membranes can drive linear aggregation of adsorbed spherical nanoparticles. *Phys. Rev. Lett.*, 108:118101, 2012.

[37] M. Terasaki, L. B. Chen, and K. Fujiwara. Microtubules and the endoplasmic reticulum are highly interdependent structures. *J. Cell Biol.*, 103:1557–1568, 1986.

[38] C. R. Hopkins, A. Gibson, M. Shipman, and K. Miller. Movement of internalized ligand-receptor complexes along a continuous endosomal reticulum. *Nature*, 346:335–339, 1990.

[39] D. Heinrich, M. Ecke, M. Jasnin, U. Engel, and G. Gerisch. Reversible membrane pearling in live cells upon destruction of the actin cortex. *Biophys. J.*, 106(5):1079–1091, mar 2014.

[40] I. Derényi, F. Jülicher, and J. Prost. Formation and interaction of membrane tubes. *Phys. Rev. Lett.*, 88(23):238101, may 2002.

[41] G. Koster, A. Cacciuto, I. Derényi, D. Frenkel, and M. Dogterom. Force barriers for membrane tube formation. *Phys. Rev. Lett.*, 94:068101, 2005.

[42] P. M. Shaklee, T. Idema, G. Koster, C. Storm, T. Schmidt, and M. Dogterom. Bidirectional membrane tube dynamics driven by nonprocessive motors. *P. Natl. Acad. Sci. USA*, 105(23):7993–7997, 2008.

[43] W. Rawicz, K. C. Olbrich, T. McIntosh, D. Needham, and E. Evans. Effect of chain length and unsaturation on elasticity of lipid bilayers. *Biophys. J.*, 79:328–339, 2000.

[44] Y. Li, R. Lipowsky, and R. Dimova. Membrane nanotubes induced by aqueous phase separation and stabilized by spontaneous curvature. *P. Natl. Acad. Sci. USA*, 108(12):4731–4736, 2011.

[45] D. Marsh. *Handbook of Lipid Bilayers*. CRC Press, second edition, 2013.

[46] L. Arleth, B. Ashok, H. Onyuksel, P. Thiyagarajan, J. Jacob, and R. P. Hjelm. Detailed structure of hairy mixed micelles formed by phosphatidylcholine and PEGylated phospholipids in aqueous media. *Langmuir*, 21(8):3279–3290, 2005.

Supporting material for "Microparticle assembly pathways on lipid membranes"

Authors: C. van der Wel, D. Heinrich, and D. J. Kraft

Supporting Videos

Videos are separately available online. Here, still images of the videos are shown together with their captions.

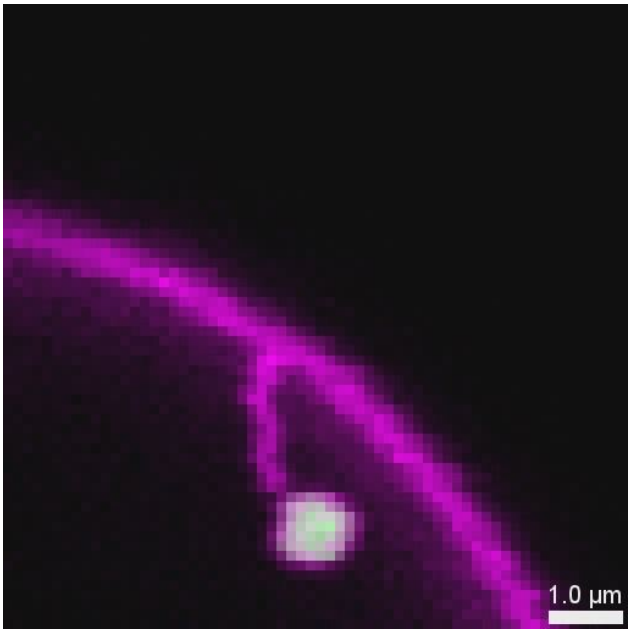

Supporting Video S1: Spontaneous tubulation induced by a 1 µm colloidal particle wrapped by a lipid membrane. The movie shows an image sequence of confocal slices of a spherical vesicle (in magenta) with colloidal particles (in green), displayed in real time.

Supporting Figures

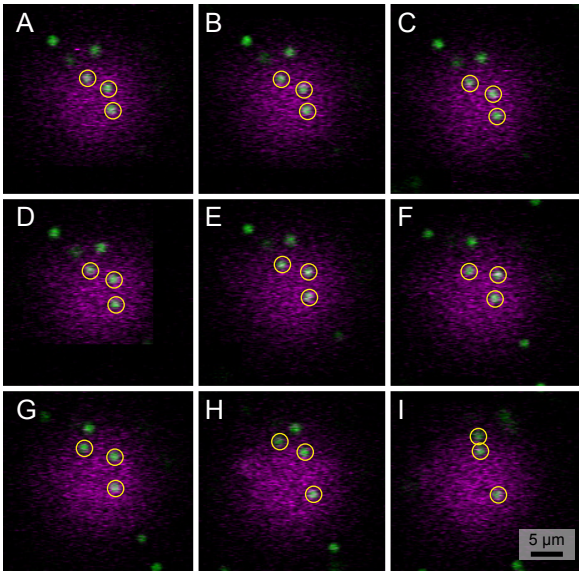

Supporting Figure S1: Time lapse of the Brownian motion of membrane-attached particles on top of a vesicle. Three tracked particles are marked with yellow circles. Frames 0, 1, 2, 4, 8, 16, 32, 64, and 128 are displayed in *(A)* to *(I)*, respectively. The frame rate is 57 Hz.

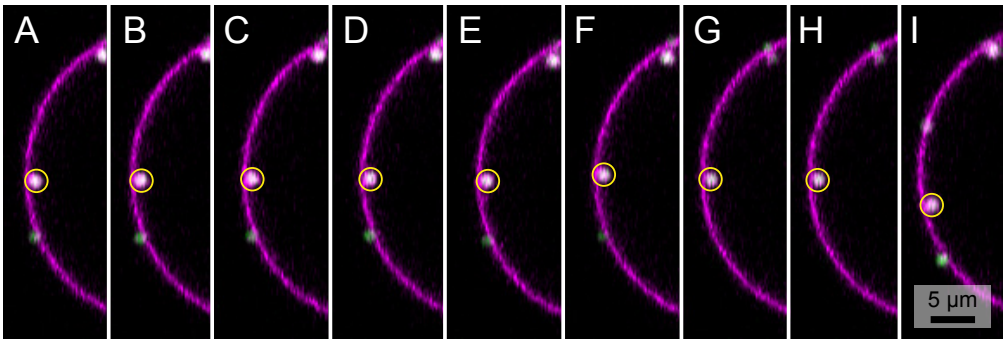

Supporting Figure S2: Time lapse of the Brownian motion of a membrane-wrapped particle in the equatorial plane of a vesicle. The particle is marked with a yellow circle. Frames 0, 1, 2, 4, 8, 16, 71, 128, and 256 are displayed in *(A)* to *(I)*, respectively. The frame rate is 57 Hz.

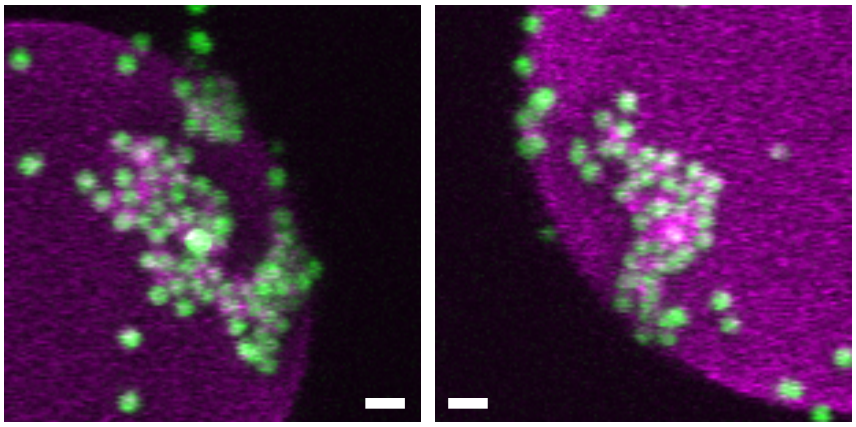

Supporting Figure S3: Confocal images of lipid vesicle-mediated particle assemblies. Both images are maximum intensity projections of three-dimensional confocal images. In this projection, the vesicle appears as a solid magenta disc. The aggregates are mediated by small lipid vesicle, as can be seen from the enhanced lipid fluorescence in between the particles. The scalebars are 2 µm.